

Spectral Cross-Domain Neural Network with Soft-adaptive Threshold Spectral Enhancement

Che Liu, Sib0 Cheng, Weiping Ding, Senior Member, IEEE, and Rossella Arcucci

Abstract—Electrocardiography (ECG) signals can be considered as multi-variable time-series. The state-of-the-art ECG data classification approaches, based on either feature engineering or deep learning techniques, treat separately spectral and time domains in machine learning systems. No spectral-time domain communication mechanism inside the classifier model can be found in current approaches, leading to difficulties in identifying complex ECG forms. In this paper, we proposed a novel deep learning model named Spectral Cross-domain neural network (SCDNN) with a new block called Soft-adaptive threshold spectral enhancement (SATSE), to simultaneously reveal the key information embedded in spectral and time domains inside the neural network. More precisely, the domain-cross information is captured by a general Convolutional neural network (CNN) backbone, and different information sources are merged by a self-adaptive mechanism to mine the connection between time and spectral domains. In SATSE, the knowledge from time and spectral domains is extracted via the Fast Fourier Transformation (FFT) with soft trainable thresholds in modified Sigmoid functions. The proposed SCDNN is tested with several classification tasks implemented on the public ECG databases *PTB-XL* and *CPSC2018*. SCDNN outperforms the state-of-the-art approaches with a low computational cost regarding a variety of metrics in all classification tasks on both databases, by finding appropriate domains from the infinite spectral mapping. The convergence of the trainable thresholds in the spectral domain is also numerically investigated in this paper. The robust performance of SCDNN provides a new perspective to exploit knowledge across deep learning models from time and spectral domains. The code repository can be found: <https://github.com/DL-WG/SCDNN-TS>

Index Terms—Deep Learning; Spectral Domain Neural Network; ECG Signal; Medical Time-Series; Cross-domain Learning

I. INTRODUCTION

Time Series has been widely studied in research fields such as physics, finance, medical, and nature language processing [1]. Due to the time dependency [2], classifying TS is different from traditional classification tasks involving image or sequence classifications without time dependencies [3]. The performance of traditional classification tasks often relies on the number of samples with proper labels [4]. In fact, well-labelled TS is often out of reach in real applications as stated in [2]. Moreover, the issue of imbalanced datasets commonly

exists in medical Time Series data [4]. As pointed out by [3], another critical challenge of time series classification involves the model generalization. It is found that different models are often required for distinct classification tasks even with the same input Time Series data [5].

The state-of-the-art time series classification approaches are either based on handcrafted feature engineering [2], [6], [7], [8], [9] or deep learning methods [10], [11], [12], [13], [14]. The former can be divided into three main categories, namely statistical feature extractions [15], [16], [17], entropy-based methods [18] and frequency-based methods [19]. After pre-processing [20], traditional machine learning classifiers such as Gradient Boosting Decision Tree (GBDT), Support Vector Machine (SVM) and Random Forest (RF) are employed to accomplish the classification tasks using handcrafted features as model input. However, the performance of FE-based methods is extremely sensitive to the quality of feature extractions on a case-to-case basis [21]. Furthermore, distinct FE methods are often required for different time series classification tasks even for the same dataset [22]. Thus, there is an insurmountable obstacle to extending specific feature engineering methods to general classification tasks.

Such challenges can be found in medical time series classification as stated in the work of [23], [24]. Electrocardiography (ECG) is a specific type of medical TS that describes the heartbeats of 12 different leads to detect various aspects of heart health [25]. In clinical applications, ECG data are widely used to diagnose cardiovascular diseases, such as myocardial infarction(MI), hypertrophy(HYP), and Conduction Disturbance(CD) [26]. A standard ECG TS consists of three waves, known as P-wave, QRS-complex and T-wave respectively [27]. As recognised in numerous researches [28], [29], [30], various cardiovascular diseases will impact these three waves, resulting in unrecognisable signals (also called repolarization in medical science). Thus identifying these abnormal signals is crucial for clinical diagnosis. In fact, successful ECG classification methods not only improve the accuracy of cardiology diagnosis, but also enable the possibility of monitoring the state of human health state using wearable devices.

Classical feature engineering-based time series classification approaches extract the features relying on different waveforms of 12-lead ECG, mostly focusing on the P-QRS-T wave [27] and RR-interval [31]. feature engineering is carried out to extract statistical, energy-based and frequency-based features which are used to classify ECG Time Series via traditional machine learning classifiers [6], [7], [8], [9]. In feature engineering based methods, the quality of the features and thus the classification performance is sensitive to the algorithms se-

Corresponding author: Sib0 Cheng (sibo.cheng@imperial.ac.uk)

Che Liu and Rossella Arcucci are with Department of Earth Science and Engineering, Imperial College London, SW7 2AZ, UK.

Che Liu is also with Data Science Institute, Department of computing, Imperial College London, SW7 2AZ, UK.

Sib0 Cheng is with Data Science Institute, Department of computing, Imperial College London, SW7 2AZ, UK.

Weiping Ding is with School of Information Science and Technology, Nantong University, Nantong 226019, China.

lected for feature computation [32]. Therefore, specific feature engineering algorithms often need to be designed for different classification tasks.

In recent years, much research attention has been given to applying deep learning approaches for ECG classification, and more generally, for time series classification tasks. For example, Convolutional Neural Networks (CNNs) have been widely employed to classify 12-lead ECG signals [11], [12], [13], [14], improving the accuracy of disease diagnosis in comparison to traditional approaches. The works of [33], [34] have used Long Short-term Memory (LSTM) [35], a variant of Recurrent Neural Network (RNN), to classify ECG pattern with imbalanced data. A wavelet layer before LSTM has been added in [36] to merge spectral domain knowledge into the Neural Network (NN). In their work, the spectral operation has been performed only on the input ECG Time Series, instead of processing deep knowledge inside the NN.

Recent works of [37], [38] have used multi-scale deep convolutional neural networks with ensemble learning to detect heart arrhythmia from 12-lead ECG. MLFB-Net [39] with CNN concatenated bidirectional GRU [40] and attention mechanism [41] has also been implemented for ECG classification where each lead ECG is treated individually. In addition, the work of [42] has tried the Transformer structure with an attention mechanism to capture latent and deep knowledge from 12-lead ECG simultaneously. However, their works only consider the ECG signals in time domain, and neglect the valuable information embedded in the spectral domain.

Recent researches, such as [37], [38], utilise multi-scale deep convolutional neural networks and ensemble learning for heart arrhythmia detection from 12-lead ECG. Another methodology, the MLFB-Net [39], employs CNN coupled with a concatenated bidirectional Gated Recurrent Unit [40] and attention mechanism [41] for ECG classification. [42] has incorporated the Transformer structure with an attention mechanism to simultaneously extract latent and deeper knowledge from 12-lead ECG, although these studies primarily focus on time domain ECG signals and may overlook spectral domain information. Our model is compared with various state-of-the-art methodologies. These include SR2-CF2 [43], a feature-based model for time series classification that utilises a genetic algorithm; EARLIEST [44], a reinforcement learning approach that outputs classification results via a trained policy network; TEASER [45], designed to handle varied-length time series early classification problems using subclassifiers; MDDNN [46], a deep learning model that combines CNN and LSTM for time series classification; ETEeTSC [47], a deep learning model that simultaneously optimises accuracy and earliness; SPN [48], a deep reinforcement learning solution for time series classification combining a deep learning backbone with a trained policy network; SPNv2 [49], a sophisticated deep reinforcement learning framework, intra-snippet spatial correlations and inter-snippet temporal correlations are integrated into concealed ECG representations, and CKNA [50], employs the strategy of imposing constraints on specific diseases, aiming to enhance the accuracy of diagnosis and early detection outcomes.

The knowledge representation on the spectral domain of

images has been introduced in the work of [51]. Following this idea, [52], [53], [54], [55] have further explored the spectral domain representation of image data on CNNs. Nevertheless, none of the aforementioned studies has established the links between the time domain and the spectral domain inside the NN. In other words, the spectral information is either processed outside the neural network [51], [52] or inside the NN but without connections to the time domain. The very recent works of [56], [57] have extended spectral domain knowledge to an infinite mapping space to approximate the proper space with Fourier Neural Operator (FNO) for image prediction tasks. In [58], FNO has been utilized to mix multi-scale features in the spectral domain to reach a more general representation of images. However, in these works, the dimension of the spectral domain is fixed and only low-frequency domain information is kept in the neural network. Hence, it is extremely challenging to obtain the proper spectral domain due to the pre-fixed threshold, and the high-frequency domain is ignored. The latter may lead to potential information loss due to the hard thresholds [59].

As discussed, although much effort has been dedicated to time series classification involved spectral knowledge, the noted algorithms suffer from the following limitations and challenges:

- 1) Current approaches either process the spectral information outside the deep learning model or treat time and spectral domains separately in the neural network. No communication between time and spectral domains inside the neural network has been performed;
- 2) When filtering information in the spectral domain, pre-selected number of spectral modes are employed, leading to potential information loss.

To overcome these bottlenecks, we propose a novel neural network structure, named Spectral Cross-domain neural network (SCDNN), that interacts the time domain and the spectral domain inside the NNs. In addition, we have developed a new soft self-adaptive threshold determination mechanism that is deployed in the Soft-adaptive Threshold Spectral Enhancement (SATSE) block of Spectral Cross-domain Neural Network (SCDNN). More precisely, this new mechanism enables SCDNN to find the optimal number of spectral modes instead of using pre-fixed thresholds as implemented in existing approaches. Furthermore, the information loss of spectral filtering can be decreased thanks to the controllable soft threshold. To verify our model's performance and versatility, four diverse ECG classification tasks are deployed. These tasks consist of 14 different cardiovascular diseases classifications on the public datasets *PTB – XL* and *CPSC2018*. SCDNN achieves substantial enhancement compared to existing time series classification models, in relation to almost all comparison metrics evaluated.

In summary, the principle contributions of our work are listed below:

- 1) We designed a novel neural network structure, named SCDNN, to establish the communication of spectral and time domains inside NNs. More precisely, Fast Fourier

Transformation (FFT) and Inverse Fast Fourier Transformation (IFFT) are added on the ResNet backbone after each Res block to learn the information in the spectral domain.

- 2) In the SATSE block of SCDNN, trainable soft thresholds in the spectral domain enable the proposed model to find optimal spectral modes and reduce the information loss compared to using pre-fixed thresholds.
- 3) The efficacy of the proposed SCDNN and SATSE has been rigorously assessed using two publicly accessible, large-scale datasets, namely *PTB – XL* and *CPSC2018*. All results attest to the superior performance of the SCDNN in cardiovascular disease classification across all four evaluation metrics.

The rest of this paper is organised as follows. Section II describes the proposed SCDNN with a detailed explanation of information processing in the spectral domain. The numerical results of the proposed network, compared to state-of-the-art approaches, on the *PTB – XL* and *CPSC2018* databases are presented in Sec III-D and III-E, respectively. We end the paper with a conclusion in Sec IV where we have also mentioned potential future works.

II. SCDNN: METHODOLOGY

In this section, we introduce the workflow of the proposed SCDNN with a special focus on the SATSE block. The proposed model is composed of ResNet18 [60] backbone, four SATSE blocks, one adaptive average pooling layer [61], one adaptive max pooling layer [62] and one fully-connected layer as displayed in Fig 1. The backbone includes 4 Res blocks (also known as residual blocks [60]). The structure of each block is depicted in Fig 2 where all Res blocks used in this study have the same structures with a different number of channels, following the standard ResNet structure [60]. Each Res block is combined with one SATSE block to form a Convolutional Fourier (ConvF) component as illustrated in Fig 2. The SATSE block enables the NN to learn from the spectral domain.

In each ConvF block, the output of SATSE will be added to the output of the Res block to avoid the information loss from spectral learning [63] as illustrated in Fig 1. Two pooling layers are applied individually on the output of the last ConvF block for dimension reduction. Two pooled features are concatenated with channel dimension, then flattened to a 1D vector before passing to the fully-connected layer for classification.

A. Res Block

Since untrainable issues have been reported for very deep neural networks [64], ResNet was proposed by [60] where skip connections between various convolutional layer were adopted to decrease the issue of information vanishing in deep layers of neural networks. A light version of ResNet, namely ResNet18 [65] is chosen in this work as the backbone. Fig 2 depicts the layout of each Res block, consisting of four 1D convolutional layers with a common kernel size and

stride as defined in [60]. The convolutional layers are employed to extract features across all channels. To enhance the gradient stabilization, a *BatchNorm* layer [66] is deployed after each convolutional layer followed by a *ReLU* [67] activation function to avoid the gradient vanishing in deep neural networks [68].

B. SATSE

In this section, we explain in details the soft adaptive threshold and the spectral learning in spectral domain. The pipeline of SATSE is illustrated in Fig 3. First, FFT is deployed in SATSE for spectral knowledge converting. The model is thus capable of capturing deep features in time domain and spectral domain simultaneously. To choose the most proper spectral domain, we make use of trainable thresholds in each SATSE block to select the spectral modes. The soft threshold mechanism is capable of avoiding information loss in modes selection since the threshold value is obtained through network back propagation. Additionally, as shown in Fig 3, a trainable weight matrix is added to establish connections among different spectral modes. Therefore, those spectral modes in different SATSE blocks are determined mutually. For the i^{th} ($i = 1, \dots, 4$) SATSE block in SCDNN, the output of the Res block is denoted as

$$\{f_{i,k}^{(j)}\} \quad \text{where} \quad \{j, k\} \in \{0, \dots, L_i - 1\} \times \{0, \dots, C_i - 1\} \quad (1)$$

In Eq (1), C_i and L_i denote the number of channels and the signal length of the i^{th} block respectively. Let \mathcal{F} and \mathcal{F}^{-1} denote the FFT and IFFT on discrete signals, the computation of spectral domain features $f_{i,k}^{S,(j)}$ of each SATSE block and each channel is performed via discrete Fourier transform,

$$f_{i,k}^{S,(j)} = \sum_{n=0}^{L_i-1} e^{-\hat{i} \frac{2\pi}{L_i} nj} f_{i,k}^{(n)}. \quad (2)$$

$$\mathcal{F}(f_{i,k}) = [f_{i,k}^{S,(j)}]_{j=0, \dots, L_i-1} \quad (3)$$

For the sake of clarity, \hat{i} denotes the imaginary unit in $e^{-\hat{i} \frac{2\pi}{L_i}}$ while the index i is referred to the index of the SATSE block. To compute the soft trainable thresholds, modified sigmoid functions in the high- and low- frequency domain are defined respectively as:

$$\sigma^L(x) = 1 - \frac{1}{1 + e^{\gamma_i(-x + \varphi_i \cdot L_i)}} \quad (4)$$

$$\sigma^H(x) = \frac{1}{1 + e^{\gamma_i(-x + \varphi_i \cdot L_i)}} \quad (5)$$

where φ_i denotes the trainable threshold ratio and γ controls the slope of the modified sigmoid function. The dual sigmoid functions σ^L and σ^H enable the SATSE block to capture knowledge in both low- and high-frequency domains. The use of soft thresholds in Eq (5) enables the NN back-propagation compared to hard threshold functions, i.e.,

$$\sigma_{\text{hard}}^L(x) = \mathbb{1}_{x > \varphi_i L_i} \quad (6)$$

$$\sigma_{\text{hard}}^H(x) = \mathbb{1}_{x \leq \varphi_i L_i}. \quad (7)$$

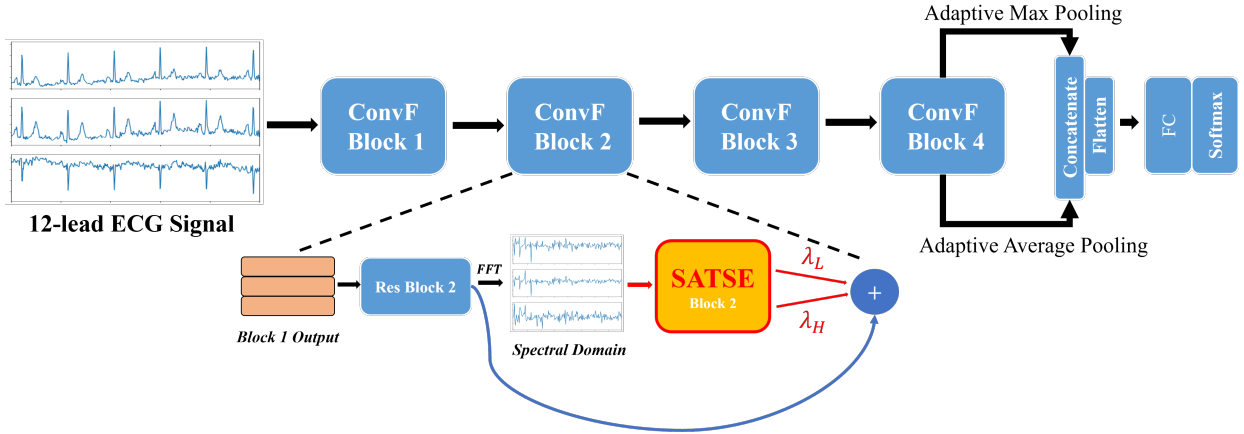


Fig. 1: Workflow of SCDNN where λ_L and λ_H denote the coefficients corresponding to low-frequency and high-frequency information

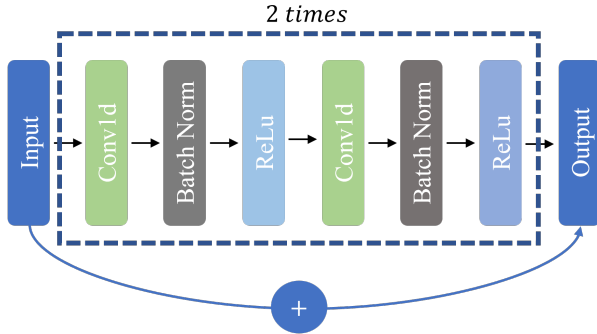


Fig. 2: Res Block Architecture

We then obtain filtered high- and low-frequency elements in the spectral domain via

$$\widehat{f}_{i,k}^{SH} = \sigma^H(k) f_{i,k}^S, \quad \widehat{f}_{i,k}^{SL} = \sigma^L(k) f_{i,k}^S. \quad (8)$$

By definition in Eq (4) and (5), when the values of γ (i.e., the slope of the sigmoid functions) are important, $\sigma^L(x) \approx \sigma_{\text{hard}}^L(x)$ and $\sigma^H(x) \approx \sigma_{\text{hard}}^H(x)$. Therefore, symmetric results can be obtained when

$$\varphi = \lambda \quad \text{and} \quad \varphi = 1 - \lambda, \quad \forall \lambda \in [0, 1] \quad (9)$$

by simply reversing the role of σ^L and σ^H . Thus the initial value of φ is set to be smaller than 0.5 in the training. To enable the communication of cross-domain and cross-block information, trainable weight matrices $W_{i,k} \in \mathbb{C}^{4, C_i}$ for different SATSE blocks and different channels are employed in the inverse Fourier transformation,

$$\widehat{f}_{i,k}^{SH} = W_{i,k} \odot \widehat{f}_{i,k}^{SH}, \quad \widehat{f}_{i,k}^{SL} = W_{i,k} \odot \widehat{f}_{i,k}^{SL} \quad (10)$$

$$f_{i,k}^{H'} = \mathcal{F}^{-1}(\widehat{f}_{i,k}^{SH}) = \frac{1}{L_i} \sum_{n=0}^{L_i-1} e^{i \frac{2\pi}{L_i} kn} \widehat{f}_{i,n}^{SH} \quad (11)$$

$$f_{i,k}^{L'} = \mathcal{F}^{-1}(\widehat{f}_{i,k}^{SL}) = \frac{1}{L_i} \sum_{n=0}^{L_i-1} e^{i \frac{2\pi}{L_i} kn} \widehat{f}_{i,n}^{SL}, \quad (12)$$

where $\{f_{i,k}^{H'}\}$ and $\{f_{i,k}^{L'}\}$ ($i = 0 \dots 3, k = 0 \dots L_i - 1$) represent the inverse Fourier sequences in time domain. The symbol \odot

denotes the element-wise multiplication in Eq (10), enabling cross spectral domain communications. Finally, the low- and high-frequency domain knowledge is converted to time domain through IFFT separately, following Eq. (11) and (12). We then obtain the output of the SATSE block O_i^{SATSE} by adding the original time domain component $\{f_{i,k}\}$ thanks to two real trainable parameters λ_L and λ_H ,

$$\begin{aligned} O_{i,k}^{\text{SATSE}} &= f_{i,k} + \lambda_L f_{i,k}^{L'} + \lambda_H f_{i,k}^{H'} \\ O_i^{\text{SATSE}} &= [O_{i,k}^{\text{SATSE}}]_{k \in \{0, \dots, C_i - 1\}}. \end{aligned} \quad (13)$$

Instead of a pre-defined threshold (e.g., [56]), trainable soft thresholds φ_i in the SATSE block avoid the information loss due to prior assumptions in SCDNN.

The training process of SCDNN is summarized in Algorithm 1.

III. EXPERIMENTS AND ANALYSIS

TABLE I: Dataset Details of PTB-XL and CPSC2018. This table is taken from [49].

Datasets	#Samples	Class	Description
PTB-XL	9528	NORM	Normal ECG
	5486	MI	Myocardial Infarction
	5250	STTC	ST/T Change
	4907	CD	Conduction Disturbance
	2655	HYP	Hypertrophy
CPSC2018	918	Normal	Normal
	1098	AF	Atrial fibrillation
	704	I-AVB	First-degree atrioventricular block
	207	LBBB	Left bundle branch block
	1695	RBBB	Right bundle branch block
	556	PAC	Premature atrial contraction
	672	PVC	Premature ventricular contraction
	825	STD	ST-segment depression
	202	STE	ST-segment elevated

A. Dataset Description

In our study, we employ two public 12-leads ECG datasets, namely PTB-XL [69] and CPSC2018 [70], to evaluate the effectiveness of our proposed SCDNN under various scenarios. The details of both datasets are displayed in Table I.

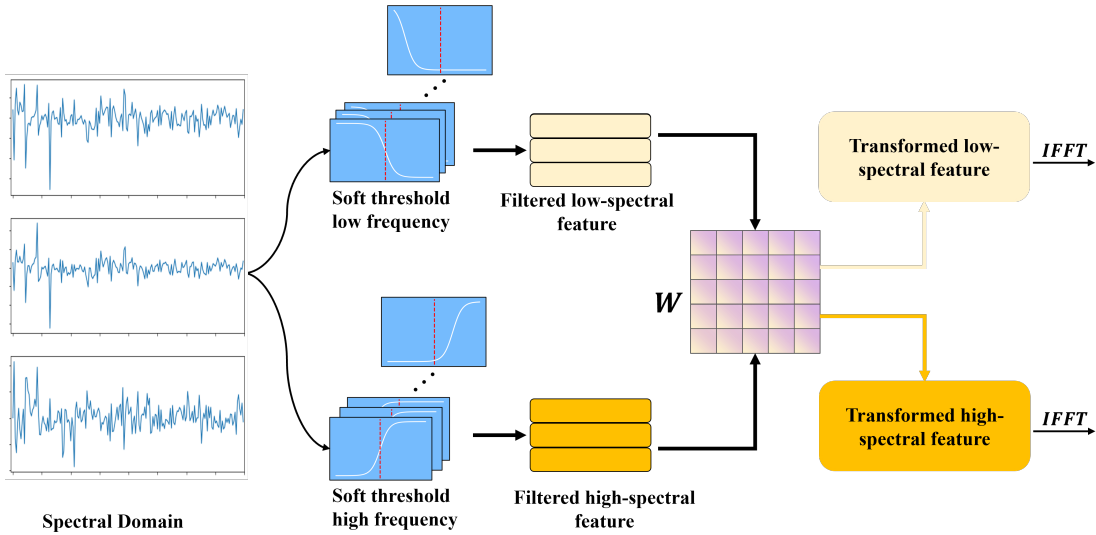


Fig. 3: SATSE Architecture

Algorithm 1 Training of SCDNN**Input:** 12 leads ECG signals and labels

- 1: Initialize model parameters
 - 2: Set Epochs number E , learning rate η , batch size m , number of sequential Res blocks r
 - 3:
 - 4: **for** $k = 0$ to E **do**
 - 5: Load ECG signals and labels with batch size
 - 6: **for** $i = 0$ to r **do**
 - 7: Forward propagation to ResBlock $_i$
 - 8: Convert the output from ResBlock $_i$ to SD via FFT (cf., Eq (2))
 - 9: Feed SD feature toward $SATSE_i$ block
 - 10: Filtering SD features individually (cf., Eq (8))
 - 11: Share mutually information on spectral domain (cf., Eq (10))
 - 12: Convert features from spectral domain to time domain via $IFFT$ (cf., Eq (11) and (12))
 - 13: Obtain the output of SATSE (cf., Eq (13))
 - 14: Adaptive average and max pooling with Concatenation
 - 15: Flatten pooled features
 - 16: Apply softmax to smooth the output probability
 - 17: Compute the model loss
 - 18: optimize model parameters with loss and η via Adams optimizer
 - 19: **end for**
 - 20: **end for**
- Output:** Probability of each label

1) *PTB-XL*: The ECG dataset under examination is substantial, encompassing 21,837 ECG signals that were accumulated from 18,885 patients during the period of October 1989 to June 1996. The collected data consists of 12-lead ECGs, each sampled at a rate of 500 Hz with a duration of 10 seconds. Furthermore, each record in this dataset is classified under

one of five primary diagnostic categories: Normal (NORM), Myocardial Infarction (MI), ST/T Change (STTC), Conduction Disturbance (CD), and Hypertrophy (HYP).

2) *CPSC2018*: This dataset, which is publicly accessible, was accumulated from 11 different hospitals as a part of the 1st China Physiological Signal Challenge. It comprises 6,877 standard 12-lead ECG records, each sampled at a rate of 500 Hz, and the duration of these records ranges from 6 to 60 seconds. The dataset is annotated with nine distinct labels, which include Atrial fibrillation (AF), First-degree atrioventricular block (I-AVB), Left bundle branch block (LBBB), Right bundle branch block (RBBB), Premature atrial contraction (PAC), Premature ventricular contraction (PVC), ST-segment depression (STD), ST-segment elevation (STE), and normal (NORM).

B. Implementation

1) *Preprocessing*: In every task, we adhere rigorously to the procedure set out in [50], [49], taking raw ECGs as inputs without any normalization process. The ECGs are resampled to a frequency of 500 Hz during dataset building [70], [69]. Given the varying signal lengths in the CPSC2018 dataset, we adopt a strategy of padding all ECGs to the maximum length encountered in the dataset, strictly adhering to the procedures outlined in [50], [49].

2) *Environment*: All experiments are implemented on a server with a 12th Intel i7-12700k CPU, 32-GB memory, and dual NVIDIA GeForce Rtx 3090 GPUs. This server runs an Ubuntu 20.04 system, and the models are implemented based on the PyTorch 1.13.1.

3) *Training Parameters Setting*: For all experimental tasks, we strictly adopt the number of epochs, batch size, initial learning rate, and weight decay rate as mentioned in [49], [50], set to 50, 32, $1e^{-4}$, and $2e^{-5}$ respectively. To establish a fair comparison with baseline methods, we select the standard *CrossEntropyLoss* [71] and Adams [72] as the loss function and the optimizer for the training process. In adherence to

the approach outlined in [49], [50], we perform a ten-fold reduction of the learning rate at the 20th epoch. Within the SATSE blocks, the initial settings of φ_i and γ_i are established at 0.4 and 0.5 per block, whereas λ_L and λ_H are initialized at 0. These parameters are subsequently updated during the network back-propagation.

C. Metrics of Performance

In order to evaluate the efficiency of the SCDNN for ECG classification, various performance measures are taken into account. While the F1 score is one of the key metrics, precision, recall, and accuracy are also critical for validating the performance of the models. All the aforementioned metrics, F1-score, Precision, Recall, and Accuracy are calculated using macro averaging.

- 1) F1-score: This is the harmonic mean of precision and recall, offering a balanced measure especially when classes are unevenly distributed.
- 2) Precision: This measures the percentage of true positive predictions among all positive predictions, indicating the level of false-positive error.
- 3) Recall: Also known as sensitivity, it shows the proportion of actual positives correctly identified, reflecting the model's ability to detect all positive cases.
- 4) Accuracy: This is the ratio of correct predictions (both positive and negative) to the total number of instances, indicating the overall correctness of the model.

D. Results on PTB-XL

An in-depth analysis of the classification results on the PTB-XL dataset, as presented in Table II, demonstrates the superiority of SCDNN over the competing methods across all metrics, including accuracy, precision, recall, and F1-score. This analysis takes into account both the mean and the standard deviation of the results, adding depth and precision to the assessment.

SCDNN emerges as the top performer in terms of accuracy, boasting a high score of 0.835 and a notably low standard deviation of 0.003. This significantly outperforms the closest competitor, SPN-V2, which achieves an accuracy of 0.805, but with a higher standard deviation of 0.021, thus highlighting the consistent accuracy of the SCDNN model.

In terms of precision, SCDNN outshines the competition once again, achieving a score of 0.804, accompanied by an impressively low standard deviation of 0.005. The next best method, SPN-V2, achieves a slightly lower precision of 0.79, but with a higher standard deviation of 0.020.

The recall metric also underlines SCDNN's superiority, with a high score of 0.787 and a small standard deviation of 0.006. CKNA, while achieving a respectable recall of 0.756, does so with a considerably higher standard deviation of 0.03.

Regarding the F1-score, which offers a balanced measure of both precision and recall, SCDNN again leads the pack, achieving a score of 0.792 and maintaining a low standard deviation of 0.005 in Table II. The closest competitors, CKNA and SPN-V2, both present a lower F1-score of 0.762, but with higher standard deviations (0.026 and 0.027 respectively).

In conclusion, the consistent high performance of SCDNN in all the metrics considered on Table II underscores its robustness and effectiveness in ECG signal classification. Furthermore, SCDNN's consistently low standard deviation scores attest to its stability and reliability as a method, making it a promising candidate for further exploration and application in the field.

E. Results on CPSC2018.

Analysing the results from the CPSC2018 dataset from Table III, it is apparent that the SCDNN method significantly outclasses the other methodologies in all examined metrics, mirroring its superior performance in the PTB-XL dataset. This consistent superior performance across disparate datasets underscores the high degree of generalizability inherent in the SCDNN method, confirming its adaptability to diverse data sources and categories.

In relation to accuracy, SCDNN achieves the highest score of 0.859, accompanied by a remarkably low standard deviation of 0.003. The nearest rival, the CKNA method, achieves an accuracy of 0.812 but with a significantly higher standard deviation of 0.013. This suggests SCDNN's superior and consistent predictive capability across varying datasets.

The trend continues in the precision metric, where SCDNN attains a superior score of 0.838, again exhibiting a low standard deviation of 0.012. The nearest competitor, the SPN method, achieves a precision of 0.762, a substantial difference that underlines the prowess of SCDNN in accurately classifying positive instances.

Furthermore, the SCDNN method surpasses all other methods in terms of recall, with an outstanding score of 0.781 and an extremely low standard deviation of 0.003. This significantly surpasses the next best recall score of 0.764 achieved by the CKNA method. This evidence suggests that SCDNN excels in correctly identifying a higher proportion of actual positive instances.

Finally, regarding the F1-score, which reflects the balance between precision and recall, SCDNN continues to outperform with a score of 0.782 and a low standard deviation of 0.003. In comparison, the second-highest F1-score is 0.764, held by the CKNA method.

In summary, the superior performance of the SCDNN method across all evaluated metrics in the CPSC2018 dataset, mirroring its performance on the PTB-XL dataset, highlights its powerful generalizability and transferability. This suggests the SCDNN method's considerable promise in the realm of ECG signal analysis.

F. Model Efficiency Analysis

For a comparative analysis of SCDNN's efficiency comparing to other benchmarks, we present Fig 4a and 5a, charting the inference time on PTB-XL and CPSC2018 datasets respectively. Further, performance metric, including accuracy, recall, and f1-score, are delineated in Fig 4b-4d and 5b-5d. An inspection of Fig 4a and 5a reveals that the SCDNN model exhibits the second lowest inference duration among all compared models, thereby conferring a significant temporal

TABLE II: Classification Results on PTB-XL. All results are inherited from [50], [49].

	Accuracy	Precision	Recall	F1-score
SR2-CF2 [43]	0.229 ± 0.003	0.227 ± 0.140	0.200 ± 0.001	0.076 ± 0.001
EARLIEST [44]	0.454 ± 0.009	0.351 ± 0.056	0.227 ± 0.007	0.188 ± 0.010
TEASER [45]	0.584 ± 0.007	0.494 ± 0.009	0.455 ± 0.009	0.461 ± 0.009
MDDNN [46]	0.733 ± 0.017	0.622 ± 0.041	0.581 ± 0.025	0.586 ± 0.027
ETEEtTSC [47]	0.744 ± 0.015	0.653 ± 0.025	0.620 ± 0.029	0.629 ± 0.027
SPN [48]	0.794 ± 0.013	0.732 ± 0.025	0.705 ± 0.031	0.710 ± 0.023
SPN-V2 [49]	0.805 ± 0.021	0.790 ± 0.020	0.744 ± 0.031	0.762 ± 0.027
CKNA [50]	0.799 ± 0.022	-	0.756 ± 0.030	0.762 ± 0.026
SCDNN	0.835 ± 0.003	0.804 ± 0.005	0.787 ± 0.006	0.792 ± 0.005

TABLE III: Results on CPSC2018. All results are inherited from [50], [49].

	Accuracy	Precision	Recall	F1-score
SR2-CF2 [43]	0.167 ± 0.009	0.579 ± 0.110	0.160 ± 0.010	0.109 ± 0.016
EARLIEST [44]	0.282 ± 0.012	0.168 ± 0.055	0.150 ± 0.015	0.114 ± 0.018
TEASER [45]	0.584 ± 0.018	0.569 ± 0.057	0.465 ± 0.017	0.480 ± 0.020
MDDNN [46]	0.585 ± 0.015	0.522 ± 0.016	0.511 ± 0.015	0.511 ± 0.015
ETEEtTSC [47]	0.733 ± 0.021	0.695 ± 0.030	0.668 ± 0.022	0.672 ± 0.026
SPN [48]	0.788 ± 0.015	0.762 ± 0.018	0.742 ± 0.014	0.745 ± 0.015
SPN-V2 [49]	0.786 ± 0.017	0.741 ± 0.027	0.724 ± 0.026	0.727 ± 0.026
CKNA [50]	0.812 ± 0.013	-	0.764 ± 0.026	0.764 ± 0.023
SCDNN	0.859 ± 0.003	0.838 ± 0.012	0.781 ± 0.003	0.782 ± 0.003

efficiency advantage in the inference phase when juxtaposed against other baselines. Meanwhile, Fig 4b-4d and 5b-5d elucidate the fact that SCDNN consistently achieves the highest performance across all three metrics, across both datasets, a testament to its superior proficiency.

Interestingly, the model that attains the highest inference speed, EARLIEST, only delivers second lowest results, highlighting the noteworthy trade-off between computational speed and performance. Nevertheless, SCDNN effectively bridges this gap, striking an optimal balance between temporal efficiency and performance metrics. As such, the empirical evidence underscores the unrivalled efficacy of SCDNN, making it a commendable choice in both time efficiency and performance arenas.

In a bid to further compare the performance characteristics of SCDNN, SPNv2, and CKNA—the two best performing baselines—we have charted the recall of each disease on both the PTB-XL and CPSC2018 datasets, as depicted in Figure 6. In the context of the PTB-XL dataset, SCDNN establishes superiority over other methodologies on CD and MI, while attaining results commensurate with other diseases. When considering the CPSC2018 dataset, SCDNN surpasses other baseline methodologies on AF, I-AVB, STD, with outcomes on remaining diseases being in the same range as other methods. These findings highlight the robust and consistent performance of the SCDNN model across various conditions and datasets, underscoring its potential as an effective tool for cardiovascular disease detection and classification.

G. Impact of Adaptive Frequency Filter

The evolution of model parameters against training Epochs is illustrated in Fig 7. Regardless the initial values, the convergence can be observed for φ_1, φ_2 and φ_3 in Fig 7(a-c). On the other hand, φ_4 converges numerically to 0 or 1

regarding different initial values as shown in Fig 7 (d). In fact, as explained in Section II-B, $\varphi_i \rightarrow 0$ and $\varphi_i \rightarrow 1$, this will lead to the same numerical outputs for the neural network by simply reversing the role of σ^L and σ^H . We also display the evolution of λ^H and λ^L accordingly in Fig 7(e,f). Regardless the initial values of φ^i , the evolution of λ^H and λ^L remains numerically stable. These results underline the robustness of the proposed SCDNN with a large range of initial parameters.

H. Ablation Study

1) *Impact of SATSE Blocks:* In the ablation study presented in Table IV, we examine the impact of varying numbers of SATSE blocks on model performance across two datasets, PTB-XL and CPSC2018. In the absence of any SATSE blocks, the model yields the lowest performance. The addition of a single SATSE block significantly enhances the model's effectiveness. The upward trend continues with the integration of two and three SATSE blocks, showing consistent improvements in all metrics. Notably, the model incorporating all four SATSE blocks achieves the highest performance on both datasets. This outcome underlines the cumulative effectiveness of SATSE blocks, indicating a directly proportional relationship between the number of SATSE blocks and model performance. Thus, SATSE blocks have been validated as a crucial component for improving model performance on both the PTB-XL and CPSC2018 datasets.

2) *Impact of Fixed Frequency Threshold:* In our investigation, replacing adaptive φ_i with fixed values ranging from 0.1 to 0.4, we observe notable performance variations on the PTB-XL and CPSC2018 datasets as demonstrated in Table V. The ablation study in Table V shows that a fixed φ_i of 0.2 delivers the highest performance across all metrics. However, performance diminishes slightly as φ_i increases beyond this

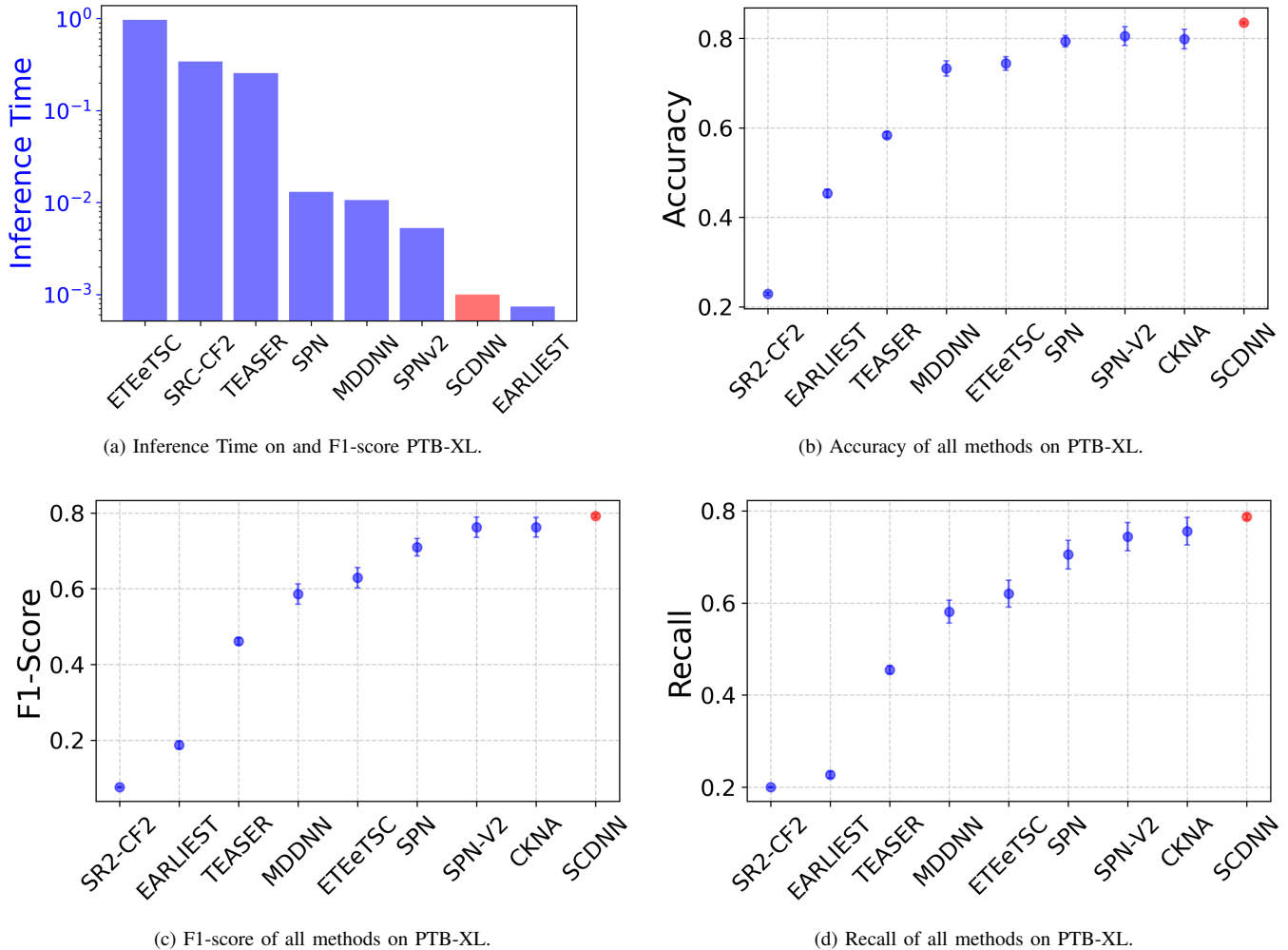


Fig. 4: Performance regarding inference time and prediction performance of SCDNN compared to baseline approaches on the PTB-XL dataset.

TABLE IV: Ablation study of the number of SATSE blocks.

SATSE Blocks	PTB-XL				CPSC2018								
	None	1	2	3	4	Accuracy	Precision	Recall	F1-score				
✓						0.711 ± 0.012	0.677 ± 0.011	0.668 ± 0.014	0.673 ± 0.013	0.727 ± 0.016	0.708 ± 0.015	0.697 ± 0.018	0.702 ± 0.017
	✓					0.754 ± 0.006	0.725 ± 0.007	0.714 ± 0.008	0.719 ± 0.008	0.776 ± 0.007	0.755 ± 0.010	0.746 ± 0.011	0.750 ± 0.011
	✓	✓				0.786 ± 0.018	0.759 ± 0.017	0.744 ± 0.020	0.751 ± 0.019	0.811 ± 0.021	0.790 ± 0.024	0.777 ± 0.025	0.783 ± 0.024
	✓	✓	✓			0.814 ± 0.004	0.786 ± 0.005	0.772 ± 0.006	0.779 ± 0.005	0.837 ± 0.005	0.819 ± 0.008	0.806 ± 0.007	0.812 ± 0.007
	✓	✓	✓	✓		0.835 ± 0.003	0.804 ± 0.005	0.787 ± 0.006	0.792 ± 0.005	0.859 ± 0.003	0.838 ± 0.012	0.781 ± 0.003	0.782 ± 0.003

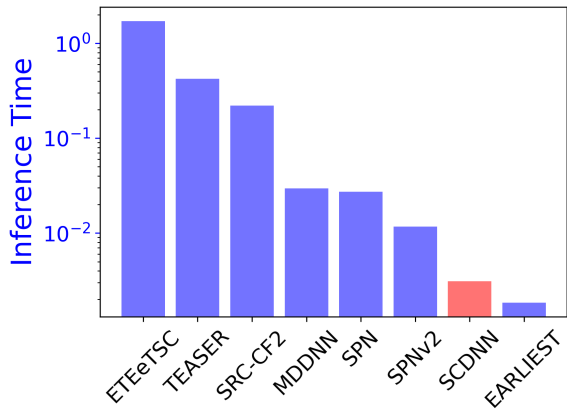
point, which underscores the sensitivity of model outcomes to the selected φ_i value. When comparing this to Tables III and II, we find that our SCDNN model with an adaptive φ_i outperforms the model using a fixed φ_i of 0.2. This superior performance of the adaptive φ_i demonstrates its capability to effectively adapt to different data variations, reinforcing the advantage of flexibility in parameter configuration.

3) *Impact of Backbone Depth*: To assess the influence of different backbone depths on the model’s performance, we chose three variants of ResNet architecture - ResNet18, ResNet34, and ResNet50 - for our experiments. The corresponding results are presented in Table VI. Surprisingly, the shallowest architecture, ResNet18, outperforms its deeper

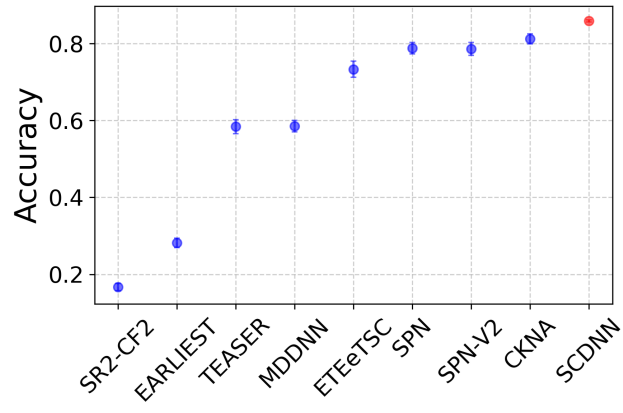
counterparts on both datasets as shown in Table VI. This suggests that a more complex model does not guarantee better performance, highlighting the importance of model depth selection for balancing accuracy and computational efficiency.

IV. CONCLUSION AND FUTURE WORK

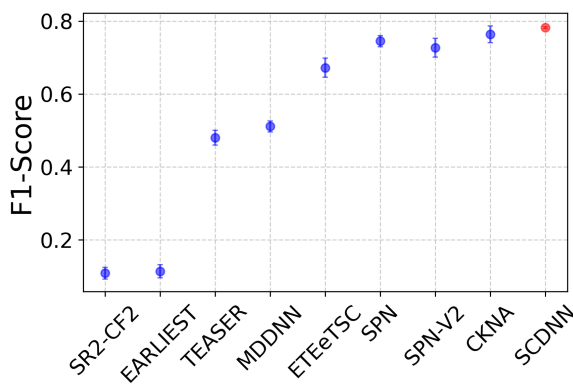
The SCDNN proposed in this study effectively fuses information from the time and spectral domains, thanks to a key architectural innovation - SATSE block. This block, equipped with trainable thresholds, adeptly filters high- and low-frequency domain information. SCDNN’s efficacy is rigorously tested on two public, large-scale, 12-lead ECG signal



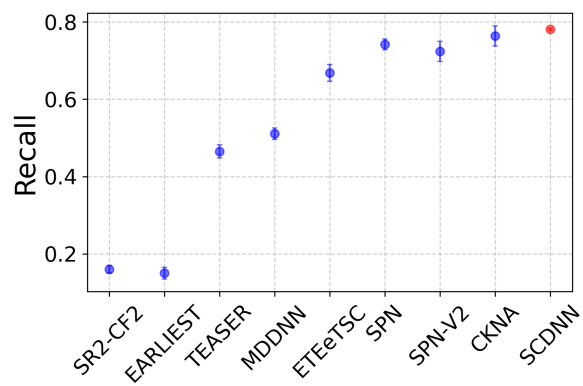
(a) Inference Time and F1-score on CPSC2018.



(b) Accuracy of all methods on CPSC2018.

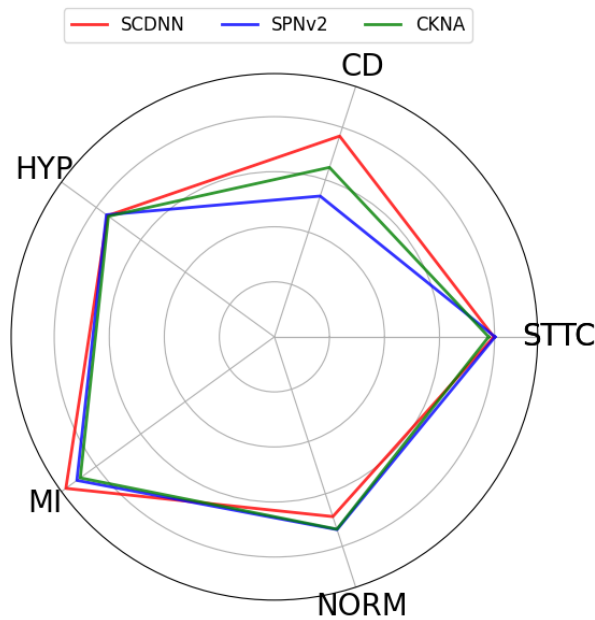


(c) F1-score of all methods on CPSC2018.

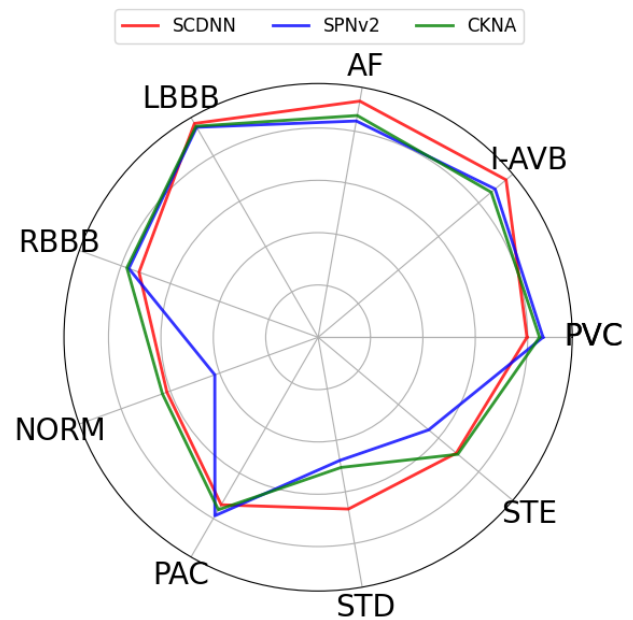


(d) Recall of all methods on CPSC2018.

Fig. 5: Performance regarding inference time and prediction performance of SCDNN compared to baseline approaches on the CPSC2018 dataset.



(a) Recall of 5 diseases on PTB-XL.



(b) Recall of 9 diseases on CPSC2018.

Fig. 6: Recall on each disease of SCDNN compared to the best two baseline.

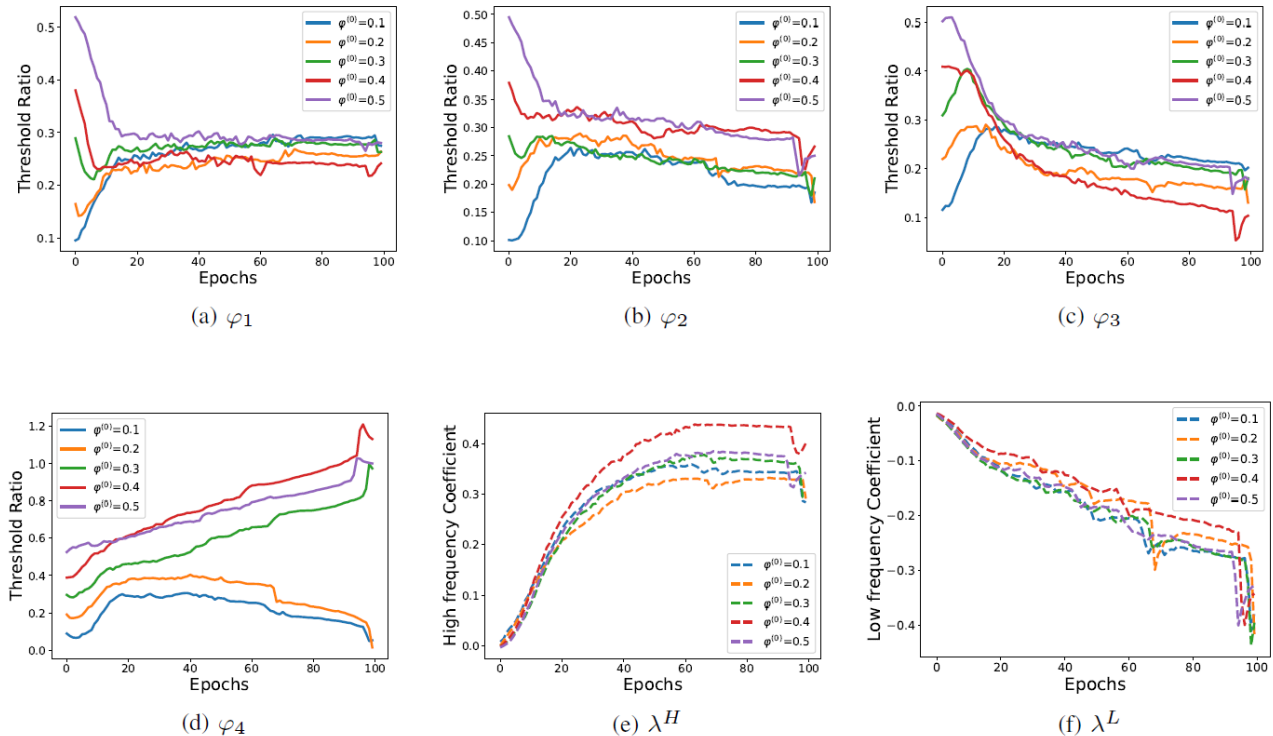


Fig. 7: Evolution of $\varphi_i, i = 1, \dots, 4, \lambda^H$ and λ^L against training Epochs with different initial values of φ_i on PTB-XL dataset.

TABLE V: Ablation study of the fixed φ_i value.

Fixed φ	PTB-XL				CPSC2018							
	0.1	0.2	0.3	0.4	Accuracy	Precision	Recall	F1-score	Accuracy	Precision	Recall	F1-score
✓					0.792 ± 0.007	0.765 ± 0.008	0.750 ± 0.010	0.757 ± 0.009	0.815 ± 0.008	0.796 ± 0.011	0.781 ± 0.012	0.789 ± 0.011
	✓				0.822 ± 0.006	0.791 ± 0.007	0.774 ± 0.008	0.781 ± 0.006	0.843 ± 0.006	0.824 ± 0.011	0.769 ± 0.006	0.771 ± 0.006
		✓			0.806 ± 0.006	0.778 ± 0.007	0.763 ± 0.008	0.770 ± 0.007	0.828 ± 0.007	0.808 ± 0.010	0.793 ± 0.009	0.800 ± 0.009
			✓		0.784 ± 0.009	0.756 ± 0.010	0.742 ± 0.011	0.749 ± 0.010	0.808 ± 0.010	0.788 ± 0.013	0.773 ± 0.012	0.780 ± 0.012

TABLE VI: Ablation study of backbone depth.

Backbone	PTB-XL				CPSC2018			
	Accuracy	Precision	Recall	F1-score	Accuracy	Precision	Recall	F1-score
ResNet18	0.835 ± 0.003	0.804 ± 0.005	0.787 ± 0.006	0.792 ± 0.005	0.859 ± 0.003	0.838 ± 0.012	0.781 ± 0.003	0.782 ± 0.003
ResNet34	0.821 ± 0.007	0.801 ± 0.009	0.784 ± 0.004	0.789 ± 0.003	0.854 ± 0.012	0.832 ± 0.008	0.776 ± 0.007	0.780 ± 0.008
ResNet50	0.818 ± 0.004	0.798 ± 0.005	0.785 ± 0.013	0.788 ± 0.011	0.851 ± 0.009	0.833 ± 0.006	0.774 ± 0.010	0.778 ± 0.005

databases covering diverse classification tasks. In comparison to existing state-of-the-art methodologies, our model shows a significant advantage across all metrics, underscoring the utility of spectral domain knowledge for minimizing convolutional layer information loss. Importantly, the SATSE’s ability to adaptively select appropriate frequency modes in the spectral domain demonstrates a tangible benefit. The crucial contribution of the SATSE is further substantiated by our comprehensive ablation studies. The SCDNN framework’s applicability extends beyond its current implementation. Its potential use in various fields like computer vision, natural language processing, speech signals, and physics systems will be further investigated. Notably, SCDNN boasts the shortest inference time, the highest performance on all metrics for the two datasets, and the lowest standard deviation values compared to other models, underscoring its impressive efficiency and effectiveness.

ACRONYMS

NN	Neural Network
ConvF	Convolutional Fourier
FFT	Fast Fourier Transformation
FNO	Fourier Neural Operator
SCDNN	Spectral Cross-domain Neural Network
RNN	Recurrent Neural Network
IFFT	Inverse Fast Fourier Transformation
CNN	Convolutional Neural Network
LSTM	Long Short-term Memory
SATSE	Soft-adaptive Threshold Spectral Enhancement
ECG	Electrocardiography
GBDT	Gradient Boosting Decision Tree
SVM	Support Vector Machine
RF	Random Forest

$f_{i,k}^{(j)}$	output of the Res block in SATSE
C_i	number of channels in the i^{th} SATSE block
L_i	signal length in the i^{th} SATSE block
$\mathcal{F}, \mathcal{F}^{-1}$	FFT and IFFT operators
$\sigma^L(\cdot), \sigma^H(\cdot)$	sigmoid functions for high- and low-frequency
γ_i	slope of the modified sigmoid function
φ_i	trainable threshold ratio
$f_{i,k}^{S,(j)}$	spectral domain features
$f_{i,k}^{SH}$	filtered high/low-frequency features
$\{f_{i,k}^{H'}\}, \{f_{i,k}^{L'}\}$	inversed Fourier sequences
$W_{i,k}$	trainable weight matrices in SATSE blocks
O_i^{SATSE}	output of the SATSE block

MAIN NOTATIONS

ACKNOWLEDGEMENT

Sibo Cheng and Rossella Arcucci acknowledges the support of the Leverhulme Centre for Wildfires, Environment and Society through the Leverhulme Trust, grant number RC-2018-023 and the EP/T000414/1 PREdictive Modelling with Quantification of UncERTainty for MultiphasE Systems (PREMIERE). Weiping Ding acknowledges the National Natural Science Foundation of China under Grant 61976120, the Natural Science Foundation of Jiangsu Province under Grant BK20231337 and the Natural Science Key Foundation of Jiangsu Education Department under Grant 21KJA510004.

REFERENCES

- [1] J. D. Hamilton, "Time series analysis." Princeton university press, 2020.
- [2] A. Bagnall, J. Lines, A. Bostrom, J. Large, and E. Keogh, "The great time series classification bake off: a review and experimental evaluation of recent algorithmic advances," *Data mining and knowledge discovery*, vol. 31, no. 3, pp. 606–660, 2017.
- [3] J. E. Ewusie, C. Soobiah, E. Blondal, J. Beyene, L. Thabane, and J. S. Hamid, "Methods, applications and challenges in the analysis of interrupted time series data: a scoping review," *Journal of Multidisciplinary Healthcare*, vol. 13, p. 411, 2020.
- [4] Q. Wen, L. Sun, F. Yang, X. Song, J. Gao, X. Wang, and H. Xu, "Time series data augmentation for deep learning: A survey," *arXiv preprint arXiv:2002.12478*, 2020.
- [5] J. Ngiam, A. Khosla, M. Kim, J. Nam, H. Lee, and A. Y. Ng, "Multimodal deep learning," in *Proceedings of the 28th international conference on machine learning (ICML-11)*, 2011, pp. 689–696.
- [6] Q. Zhao and L. Zhang, "Ecg feature extraction and classification using wavelet transform and support vector machines," in *2005 International Conference on Neural Networks and Brain*, vol. 2. IEEE, 2005, pp. 1089–1092.
- [7] M. Kallas, C. Francis, L. Kanaan, D. Merheb, P. Honeine, and H. Amoud, "Multi-class svm classification combined with kernel pca feature extraction of ecg signals," in *2012 19th International Conference on Telecommunications (ICT)*. IEEE, 2012, pp. 1–5.
- [8] T. Li and M. Zhou, "Ecg classification using wavelet packet entropy and random forests," *Entropy*, vol. 18, no. 8, p. 285, 2016.
- [9] M. Kropf, D. Hayn, and G. Schreier, "Ecg classification based on time and frequency domain features using random forests," in *2017 Computing in Cardiology (CinC)*. IEEE, 2017, pp. 1–4.
- [10] H. Ismail Fawaz, G. Forestier, J. Weber, L. Idoumghar, and P.-A. Muller, "Deep learning for time series classification: a review," *Data mining and knowledge discovery*, vol. 33, no. 4, pp. 917–963, 2019.
- [11] A. Mostayed, J. Luo, X. Shu, and W. Wee, "Classification of 12-lead ecg signals with bi-directional lstm network," *arXiv preprint arXiv:1811.02090*, 2018.
- [12] T. Yang, L. Yu, Q. Jin, L. Wu, and B. He, "Localization of origins of premature ventricular contraction by means of convolutional neural network from 12-lead ecg," *IEEE Transactions on Biomedical Engineering*, vol. 65, no. 7, pp. 1662–1671, 2017.
- [13] Z. Liu, X. Meng, J. Cui, Z. Huang, and J. Wu, "Automatic identification of abnormalities in 12-lead ecgs using expert features and convolutional neural networks," in *2018 International Conference on Sensor Networks and Signal Processing (SNSP)*. IEEE, 2018, pp. 163–167.
- [14] M. Kachuee, S. Fazeli, and M. Sarrafzadeh, "Ecg heartbeat classification: A deep transferable representation," in *2018 IEEE international conference on healthcare informatics (ICHI)*. IEEE, 2018, pp. 443–444.
- [15] T. W. Anderson, *The statistical analysis of time series*. John Wiley & Sons, 2011.
- [16] X. Luo, Y. Yuan, S. Chen, N. Zeng, and Z. Wang, "Position-transitional particle swarm optimization-incorporated latent factor analysis," *IEEE Transactions on Knowledge and Data Engineering*, vol. 34, no. 8, pp. 3958–3970, 2020.
- [17] X. Luo, H. Wu, Z. Wang, J. Wang, and D. Meng, "A novel approach to large-scale dynamically weighted directed network representation," *IEEE Transactions on Pattern Analysis and Machine Intelligence*, vol. 44, no. 12, pp. 9756–9773, 2021.
- [18] B. D. Fulcher and N. S. Jones, "Highly comparative feature-based time-series classification," *IEEE Transactions on Knowledge and Data Engineering*, vol. 26, no. 12, pp. 3026–3037, 2014.
- [19] J. Lines and A. Bagnall, "Time series classification with ensembles of elastic distance measures," *Data Mining and Knowledge Discovery*, vol. 29, no. 3, pp. 565–592, 2015.
- [20] C. Faloutsos, M. Ranganathan, and Y. Manolopoulos, "Fast subsequence matching in time-series databases," *ACM Sigmod Record*, vol. 23, no. 2, pp. 419–429, 1994.
- [21] D. Halliday, J. Rosenberg, A. Amjad, P. Breeze, B. Conway, S. Farmer, et al., "A framework for the analysis of mixed time series/point process data-theory and application to the study of physiological tremor, single motor unit discharges and electromyograms," *Progress in biophysics and molecular biology*, vol. 64, no. 2, p. 237, 1995.
- [22] G. E. Box, G. M. Jenkins, G. C. Reinsel, and G. M. Ljung, "Time series analysis: forecasting and control." John Wiley & Sons, 2015.
- [23] K. Sternickel, "Automatic pattern recognition in ecg time series," *Computer methods and programs in biomedicine*, vol. 68, no. 2, pp. 109–115, 2002.
- [24] M. C. Chuah and F. Fu, "Ecg anomaly detection via time series analysis," in *Frontiers of High Performance Computing and Networking ISPA 2007 Workshops: ISPA 2007 International Workshops SSDSN, UPWN, WISH, SGC, ParDMCom, HIPCoMB, and IST-AWSN Niagara Falls, Canada, August 28-September 1, 2007 Proceedings 5*. Springer, 2007, pp. 123–135.
- [25] A. W. van't Hof, A. Liem, M.-J. de Boer, F. Zijlstra, Z. M. I. S. Group, et al., "Clinical value of 12-lead electrocardiogram after successful reperfusion therapy for acute myocardial infarction," *The Lancet*, vol. 350, no. 9078, pp. 615–619, 1997.
- [26] E. A. Ashley, V. Raxwal, and V. Froelicher, "An evidence-based review of the resting electrocardiogram as a screening technique for heart disease," *Progress in cardiovascular diseases*, vol. 44, no. 1, pp. 55–67, 2001.
- [27] J. W. Hurst, "Naming of the waves in the ecg, with a brief account of their genesis," *Circulation*, vol. 98, no. 18, pp. 1937–1942, 1998.
- [28] P. M. Rautaharju, B. Surawicz, and L. S. Gettes, "Aha/accl/hrs recommendations for the standardization and interpretation of the electrocardiogram: part iv: the st segment, t and u waves, and the qt interval a scientific statement from the american heart association electrocardiography and arrhythmias committee, council on clinical cardiology; the american college of cardiology foundation; and the heart rhythm society endorsed by the international society for computerized electrocardiology," *Journal of the American College of Cardiology*, vol. 53, no. 11, pp. 982–991, 2009.
- [29] D. De Bacquer, G. De Backer, M. Kornitzer, and H. Blackburn, "Prognostic value of ecg findings for total, cardiovascular disease, and coronary heart disease death in men and women," *Heart*, vol. 80, no. 6, pp. 570–577, 1998.
- [30] B. J. Maron, R. A. Friedman, P. Kligfield, B. D. Levine, S. Viskin, B. R. Chaitman, P. M. Okin, J. P. Saul, L. Salberg, G. F. Van Hare, et al., "Assessment of the 12-lead ecg as a screening test for detection of cardiovascular disease in healthy general populations of young people (12–25 years of age) a scientific statement from the american heart association and the american college of cardiology," *Circulation*, vol. 130, no. 15, pp. 1303–1334, 2014.
- [31] T. E. Brown, L. A. Beightol, J. Koh, and D. L. Eckberg, "Important influence of respiration on human rr interval power spectra is largely ignored," *Journal of Applied Physiology*, vol. 75, no. 5, pp. 2310–2317, 1993.

- [32] J. Ma, X. Jiang, A. Fan, J. Jiang, and J. Yan, "Image matching from handcrafted to deep features: A survey," *International Journal of Computer Vision*, vol. 129, no. 1, pp. 23–79, 2021.
- [33] B. Hou, J. Yang, P. Wang, and R. Yan, "Lstm-based auto-encoder model for ecg arrhythmias classification," *IEEE Transactions on Instrumentation and Measurement*, vol. 69, no. 4, pp. 1232–1240, 2019.
- [34] J. Gao, H. Zhang, P. Lu, and Z. Wang, "An effective lstm recurrent network to detect arrhythmia on imbalanced ecg dataset," *Journal of healthcare engineering*, vol. 2019, 2019.
- [35] S. Hochreiter and J. Schmidhuber, "Long short-term memory," *Neural computation*, vol. 9, no. 8, pp. 1735–1780, 1997.
- [36] Ö. Yildirim, "A novel wavelet sequence based on deep bidirectional lstm network model for ecg signal classification," *Computers in biology and medicine*, vol. 96, pp. 189–202, 2018.
- [37] R. Wang, J. Fan, and Y. Li, "Deep multi-scale fusion neural network for multi-class arrhythmia detection," *IEEE journal of biomedical and health informatics*, vol. 24, no. 9, pp. 2461–2472, 2020.
- [38] E. Prabhakararao and S. Dandapat, "Multi-scale convolutional neural network ensemble for multi-class arrhythmia classification," *IEEE Journal of Biomedical and Health Informatics*, 2021.
- [39] J. Zhang, D. Liang, A. Liu, M. Gao, X. Chen, X. Zhang, and X. Chen, "Mlbf-net: a multi-lead-branch fusion network for multi-class arrhythmia classification using 12-lead ecg," *IEEE Journal of Translational Engineering in Health and Medicine*, vol. 9, pp. 1–11, 2021.
- [40] R. Dey and F. M. Salem, "Gate-variants of gated recurrent unit (gru) neural networks," in *2017 IEEE 60th international midwest symposium on circuits and systems (MWSCAS)*. IEEE, 2017, pp. 1597–1600.
- [41] A. Vaswani, N. Shazeer, N. Parmar, J. Uszkoreit, L. Jones, A. N. Gomez, Ł. Kaiser, and I. Polosukhin, "Attention is all you need," *Advances in neural information processing systems*, vol. 30, 2017.
- [42] X. Li, C. Li, Y. Wei, Y. Sun, J. Wei, X. Li, and B. Qian, "Bat: Beat-aligned transformer for electrocardiogram classification," in *2021 IEEE International Conference on Data Mining (ICDM)*. IEEE, 2021, pp. 320–329.
- [43] U. Mori, A. Mendiburu, S. Dasgupta, and J. A. Lozano, "Early classification of time series by simultaneously optimizing the accuracy and earliness," *IEEE transactions on neural networks and learning systems*, vol. 29, no. 10, pp. 4569–4578, 2017.
- [44] T. Hartvigsen, C. Sen, X. Kong, and E. Rundensteiner, "Adaptive-halting policy network for early classification," in *Proceedings of the 25th ACM SIGKDD International Conference on Knowledge Discovery & Data Mining*, 2019, pp. 101–110.
- [45] P. Schäfer and U. Leser, "Teaser: early and accurate time series classification," *Data mining and knowledge discovery*, vol. 34, no. 5, pp. 1336–1362, 2020.
- [46] H.-S. Huang, C.-L. Liu, and V. S. Tseng, "Multivariate time series early classification using multi-domain deep neural network," in *2018 IEEE 5th International Conference on Data Science and Advanced Analytics (DSAA)*. IEEE, 2018, pp. 90–98.
- [47] M. Rußwurm, S. Lefevre, N. Courty, R. Emonet, M. Körner, and R. Tavenard, "End-to-end learning for early classification of time series," *arXiv preprint arXiv:1901.10681*, 2019.
- [48] Y. Huang, G. G. Yen, and V. S. Tseng, "Snippet policy network for multi-class varied-length ecg early classification," *IEEE Transactions on Knowledge & Data Engineering*, vol. 35, no. 06, pp. 6349–6361, 2023.
- [49] Y. Huang and Yen, "Snippet policy network v2: Knee-guided neuroevolution for multi-lead ecg early classification," *IEEE Transactions on Neural Networks and Learning Systems*, 2022.
- [50] Y. Huang, G. G. Yen, and V. S. Tseng, "A novel constraint-based knee-guided neuroevolutionary algorithm for context-specific ecg early classification," *IEEE Journal of Biomedical and Health Informatics*, vol. 26, no. 11, pp. 5394–5405, 2022.
- [51] O. Rippel, J. Snoek, and R. P. Adams, "Spectral representations for convolutional neural networks," *Advances in neural information processing systems*, vol. 28, 2015.
- [52] L. Yi, H. Su, X. Guo, and L. J. Guibas, "Syncspeccnn: Synchronized spectral cnn for 3d shape segmentation," in *Proceedings of the IEEE Conference on Computer Vision and Pattern Recognition*, 2017, pp. 2282–2290.
- [53] X.-H. Han, B. Shi, and Y. Zheng, "Ssf-cnn: Spatial and spectral fusion with cnn for hyperspectral image super-resolution," in *2018 25th IEEE International Conference on Image Processing (ICIP)*. IEEE, 2018, pp. 2506–2510.
- [54] L. Mou and X. X. Zhu, "Learning to pay attention on spectral domain: A spectral attention module-based convolutional network for hyperspectral image classification," *IEEE Transactions on Geoscience and Remote Sensing*, vol. 58, no. 1, pp. 110–122, 2019.
- [55] A. M. Alqudah, "Aoct-net: a convolutional network automated classification of multiclass retinal diseases using spectral-domain optical coherence tomography images," *Medical & biological engineering & computing*, vol. 58, no. 1, pp. 41–53, 2020.
- [56] Z. Li, N. Kovachki, K. Azizzadenesheli, B. Liu, K. Bhattacharya, A. Stuart, and A. Anandkumar, "Fourier neural operator for parametric partial differential equations," *arXiv preprint arXiv:2010.08895*, 2020.
- [57] J. Pathak, S. Subramanian, P. Harrington, S. Raja, A. Chattopadhyay, M. Mardani, T. Kurth, D. Hall, Z. Li, K. Azizzadenesheli, et al., "Fourcastnet: A global data-driven high-resolution weather model using adaptive fourier neural operators," *arXiv preprint arXiv:2202.11214*, 2022.
- [58] Y. Rao, W. Zhao, Z. Zhu, J. Lu, and J. Zhou, "Global filter networks for image classification," *Advances in Neural Information Processing Systems*, vol. 34, 2021.
- [59] M. Tanter, J.-L. Thomas, and M. Fink, "Time reversal and the inverse filter," *The Journal of the Acoustical Society of America*, vol. 108, no. 1, pp. 223–234, 2000.
- [60] K. He, X. Zhang, S. Ren, and J. Sun, "Deep residual learning for image recognition," in *Proceedings of the IEEE conference on computer vision and pattern recognition*, 2016, pp. 770–778.
- [61] Y. Liu, Y.-M. Zhang, X.-Y. Zhang, and C.-L. Liu, "Adaptive spatial pooling for image classification," *Pattern Recognition*, vol. 55, pp. 58–67, 2016.
- [62] M. Cho, J. Sun, O. Duchenne, and J. Ponce, "Finding matches in a haystack: A max-pooling strategy for graph matching in the presence of outliers," in *Proceedings of the IEEE Conference on Computer Vision and Pattern Recognition*, 2014, pp. 2083–2090.
- [63] P. Duhamel and M. Vetterli, "Fast fourier transforms: a tutorial review and a state of the art," *Signal processing*, vol. 19, no. 4, pp. 259–299, 1990.
- [64] R. K. Srivastava, K. Greff, and J. Schmidhuber, "Training very deep networks," *Advances in neural information processing systems*, vol. 28, 2015.
- [65] K. He, X. Zhang, S. Ren, and J. Sun, "Identity mappings in deep residual networks," in *European conference on computer vision*. Springer, 2016, pp. 630–645.
- [66] S. Ioffe and C. Szegedy, "Batch normalization: Accelerating deep network training by reducing internal covariate shift," in *International conference on machine learning*. PMLR, 2015, pp. 448–456.
- [67] B. Xu, N. Wang, T. Chen, and M. Li, "Empirical evaluation of rectified activations in convolutional network," *arXiv preprint arXiv:1505.00853*, 2015.
- [68] S. Hochreiter, Y. Bengio, P. Frasconi, J. Schmidhuber, et al., "Gradient flow in recurrent nets: the difficulty of learning long-term dependencies," 2001.
- [69] P. Wagner, N. Strodthoff, R.-D. Boussejot, D. Kreisler, F. I. Lunze, W. Samek, and T. Schaeffter, "Ptb-xl, a large publicly available electrocardiography dataset," *Scientific data*, vol. 7, no. 1, pp. 1–15, 2020.
- [70] F. Liu, C. Liu, L. Zhao, X. Zhang, X. Wu, X. Xu, Y. Liu, C. Ma, S. Wei, Z. He, et al., "An open access database for evaluating the algorithms of electrocardiogram rhythm and morphology abnormality detection," *Journal of Medical Imaging and Health Informatics*, vol. 8, no. 7, pp. 1368–1373, 2018.
- [71] P.-T. De Boer, D. P. Kroese, S. Mannor, and R. Y. Rubinstein, "A tutorial on the cross-entropy method," *Annals of operations research*, vol. 134, no. 1, pp. 19–67, 2005.
- [72] J. Snoek, H. Larochelle, and R. P. Adams, "Practical bayesian optimization of machine learning algorithms," in *Proceedings of the 25th International Conference on Neural Information Processing Systems-Volume 2*, 2012, pp. 2951–2959.